Adsorbate-substrate charge transfer and electron-hole correlation at adsorbate/metal interfaces

M. Häming,[1] A. Schöll,[1,2,*] E. Umbach,[3] and F. Reinert[1,2]

[1]*Universität Würzburg, Experimentelle Physik VII and Röntgen Research Center for Complex Material Systems (RCCM), 97074 Würzburg, Germany*

[2]*Karlsruher Institut für Technologie (KIT), Gemeinschaftslabor für Nanoanalytik, 76186 Karlsruhe, Germany*

[3]*Karlsruher Institut für Technologie (KIT), 76021 Karlsruhe, Germany*

(Received 20 March 2012; revised manuscript received 17 May 2012; published 19 June 2012)

The interaction and charge transfer at adsorbate/metal interfaces are studied with high-resolution core level and valence band photoelectron spectroscopy (PES) and near edge x-ray absorption fine structure spectroscopy. Various multilayer and monolayer films of different organic molecules on Ag(111) surfaces are investigated systematically. Distinct spectral features are observed in the PES spectra of the monolayer films which can be attributed to the interface interaction and charge transfer. Moreover, it is shown that these features are significant indications for the hybridization of adsorbate and substrate wave functions at the interface. This is related to a metallic character of the first adsorbate layer, which can be observed with various spectroscopic techniques.

DOI: 10.1103/PhysRevB.85.235132 PACS number(s): 73.20.−r, 73.61.Ph, 73.40.Ns

I. INTRODUCTION

Photoelectron (PE) spectroscopy and near edge x-ray absorption fine structure (NEXAFS) spectroscopy are well-established techniques for studying the electronic structure of thin films, surfaces, and interfaces. Many studies have been focused on the interface interaction between thin adsorbate films and metal substrates.[1–8] It has been found that in general the interface interaction is weak for molecular adsorbate films on Au surfaces whereas it is significantly stronger for less noble metal surfaces (e.g., Ag, Cu, or Ru surfaces).[9–18] This becomes evident when comparing the PE and NEXAFS spectra of monolayer (ML) films of the same adsorbate on different metal surfaces.[9,19] Significant and characteristic spectral features have been observed for ML films of large organic molecules on Ag and Cu surfaces (e.g., for PTCDA, NTCDA, and phthalocyanine ML films). Particularly, differential peak shifts, broadening of spectral features, and significant changes of the satellite structure have been observed compared to the spectra of the multilayer films.[6,16,19,20] However, a detailed understanding of these spectral features and the adsorbate-substrate interaction has not been established yet.

Some fundamental aspects of the interaction at organic-metal interfaces are studied systematically in the following by investigating different molecular thin films on the Ag(111) surface. Four different molecules are chosen, which can be considered as derivatives of 3,4,9,10–perylene tetracarboxylic dianhydride (PTCDA), a standard molecule for surface and interface investigations. The molecular size and the electronegativity of the functional group is varied by choosing two small molecules, namely 3,3′,4,4′–benzophenone tetracarboxylic dianhydride (BTCDA) and 3,3′,4,4′–benzophenone tetracarboxylic diimide (BTCDI), and two large molecules, namely PTCDA and 3,4,9,10–perylene tetracarboxylic diimide (PTCDI). DFT calculations with a density-Gaussian-type triple-zeta-split-valence + polarization basis set (DGTZVP) indicate a decrease of the electronic gap of the free molecules in this series from BTCDA to PTCDI,[21] which suggests an increase of the adsorbate-substrate interaction to first order.

In the first step the PE spectra of the multilayer films are compared to those of the ML films and the trends in ML spectra from BTCDA to PTCDI are discussed. It will be shown that the interface interaction leads also to significant modifications of the PE and NEXAFS spectra. In the second step the core level spectra will be discussed with respect to adsorbate-substrate charge transfer. In this context the approach developed by Gunnarsson and Schönhammer[12,22–26] for adsorbates on metal surfaces and by Sawatzky *et al*. and others for transition metal compounds[27–37] is applied here to the interface problem and related to simplified considerations within the framework of the single-impurity Newns-Anderson model (SINAM). This provides valuable information on fundamental properties of the electronic structure at the adsorbate-substrate interface.

II. EXPERIMENTAL DETAILS

High-resolution core and valence level photoelectron spectroscopy (PES) data were recorded at the Berlin Electron Storage Ring Society for Synchrotron Radiation (BESSY II) at the UE52–PGM undulator beamline ($E/\Delta E > 14\,000$ at 400 eV photon energy, with cff = 10 and 20 μm exit slit).[38] For the PES experiments the setup was adjusted to normal emission geometry with 56° angle of incidence with respect to the surface normal and p-polarized light. The SCIENTA R4000 electron analyzer was operated with a constant pass energy of 50 eV and 300 μm entrance slit, resulting in an energy resolution of $\Delta E = 35$ meV. After each measurement the energy scale was carefully calibrated to the Ag $3d_{5/2}$ and Ag $3d_{3/2}$ photoemission lines or the Fermi edge, respectively, resulting in an absolute accuracy of the energy scale of better than 30 meV.[39] For the NEXAFS and resonant Auger Raman spectra the setup was adjusted to 70° angle of incidence with respect to the surface normal and the polarization of the incoming x-ray light was adjusted by the undulator. The NEXAFS spectra were recorded with a homemade partial electron yield detector with 150 V and 300 V retard voltage, respectively.

The Ag(111) substrate was cleaned by several sputter and annealing cycles, which resulted in a well-ordered, clean substrate (as derived from LEED and PES). The organic

films were prepared at room temperature from powder (two times sublimated for purification) by organic molecular beam deposition from a homemade Knudsen cell at a pressure better than 1×10^{-8} mbar. The evaporation temperature was 120 °C (BTCDA), 200 °C (BTCDI), 380 °C (PTCDA), and 400 °C (PTCDI). The BTCDA, BTCDI, PTCDA, and PTCDI multilayer films were cooled to temperatures between −100 °C and −70 °C during preparation and measurements for the sake of smooth films. The PTCDA and PTCDI ML films were obtained by annealing a multilayer film for 5 min at 295 °C. The BTCDA ML films were prepared by annealing a multilayer sample for 5 min at 60 °C. For the BTCDI ML films several few minutes long annealing cycles were necessary with temperatures around 110 °C. The thickness of the ML films was verified by comparison of the peak areas of the core level signals to the PTCDA bench mark. The thickness of the multilayer films was estimated from the evaporation time and the attenuation of the Ag 3d photoemission lines.

The samples were carefully checked for radiation damage and spurious adsorbates. In order to minimize any effects from the irradiation, the light spot was stepwise scanned over the sample, and several spectra were averaged to obtain better statistics. In the following a power-law background was subtracted from all core level spectra, and a Shirley background in case of the ML data. The NEXAFS spectra were normalized to the ring current and to the flux curve, which was recorded separately using a clean substrate under the same conditions.[39]

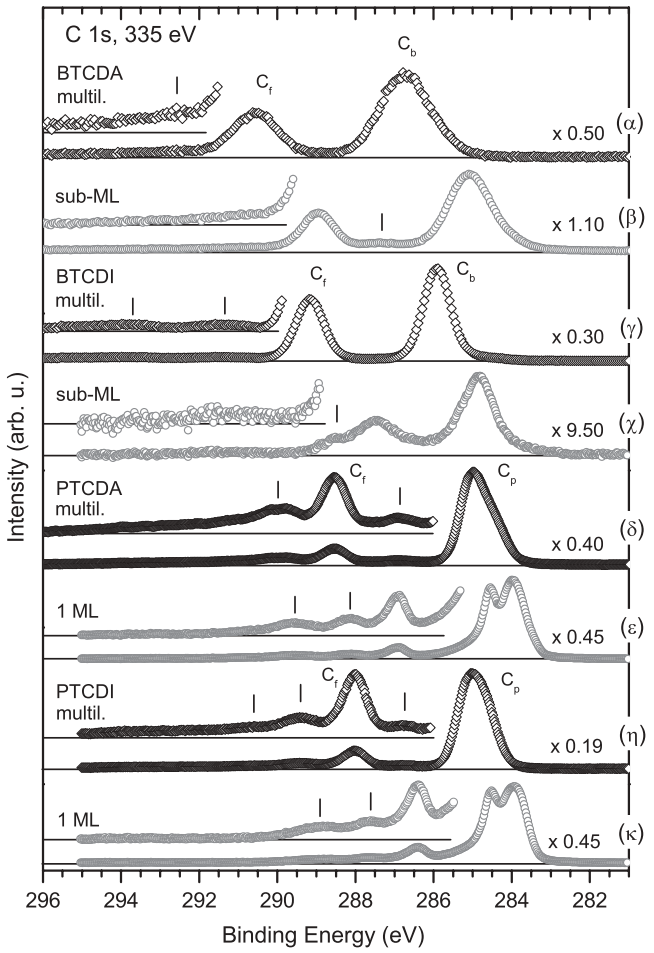

FIG. 1. Comparison of C 1*s* spectra of multilayer (black) and ML films (gray) of BTCDA (α,β), BTCDI (γ,χ), PTCDA (δ,ϵ), and PTCDI (η,κ) on Ag(111). All spectra are normalized to the background and an exponential background was subtracted; a Shirley background was subtracted in case of the 1 ML data. The satellite signal is additionally shown on a ×3.5 expanded intensity scale.

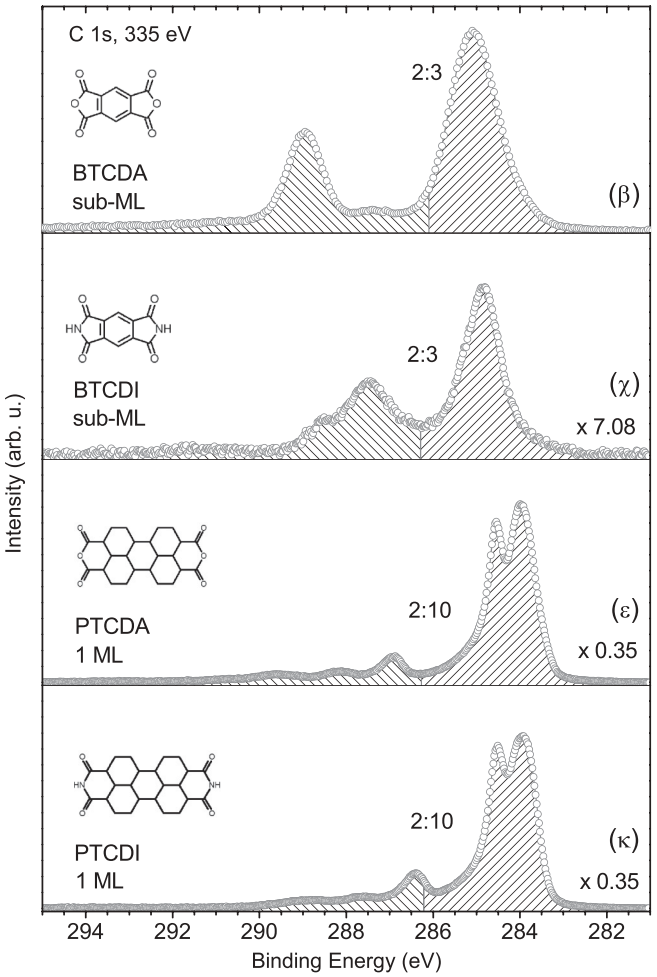

FIG. 2. Comparison of the intensities of the C 1*s* spectra of a BTCDA (β), BTCDI (χ), PTCDA (ϵ), and a PTCDI (κ) ML film on Ag(111). The ratio of the hatched areas corresponds to the stoichiometric ratio between the carbon species in the functional group and those in the molecular core, which is indicated on top of each spectrum.

III. CORE LEVEL PHOTOELECTRON SPECTROSCOPY

The model discussed in Sec. IV B is based on a comprehensive and systematic PES investigation of different adsorbate films. For this purpose all core level spectra of the BTCDA, BTCDI, PTCDA, and PTCDI multilayer and ML films are shown in Figs. 1–4, and the binding energy positions of the peak maxima are listed in Table I. These spectra have been discussed in detail in Ref. 21, where it has been shown explicitly that well-ordered films of nondissociated and intact molecules were prepared. Hence, the spectral features of interest can be attributed directly to the interface interaction. The systematic and general trends in this series of core

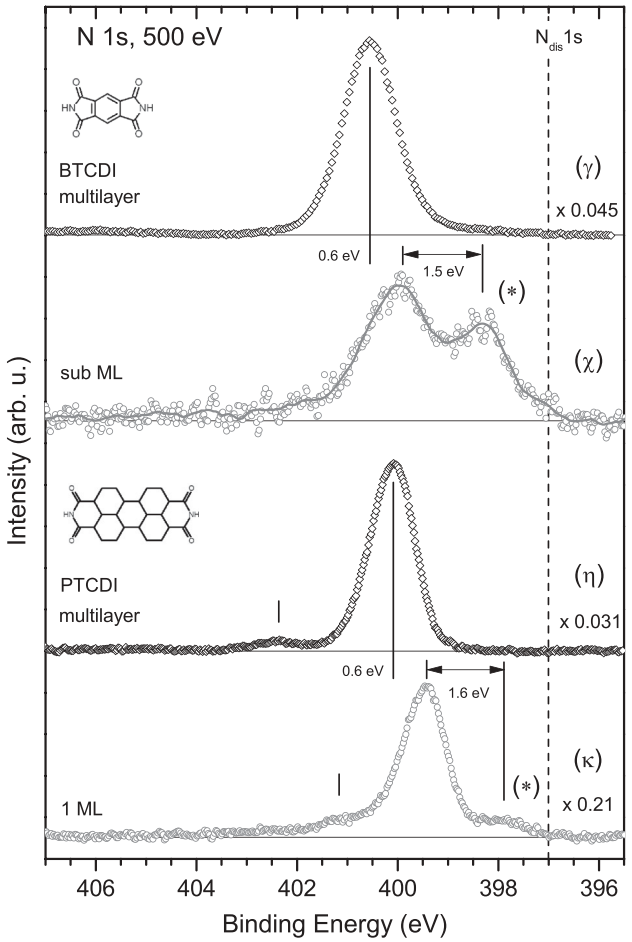

FIG. 3. Comparison of the N 1*s* spectra of multilayer (black) and ML films (gray) of BTCDI (γ,χ) and PTCDI (η,κ) on Ag(111). The energy position of dissociated nitrogen on different noble metal surfaces is marked by a vertical line.[11,48–50]

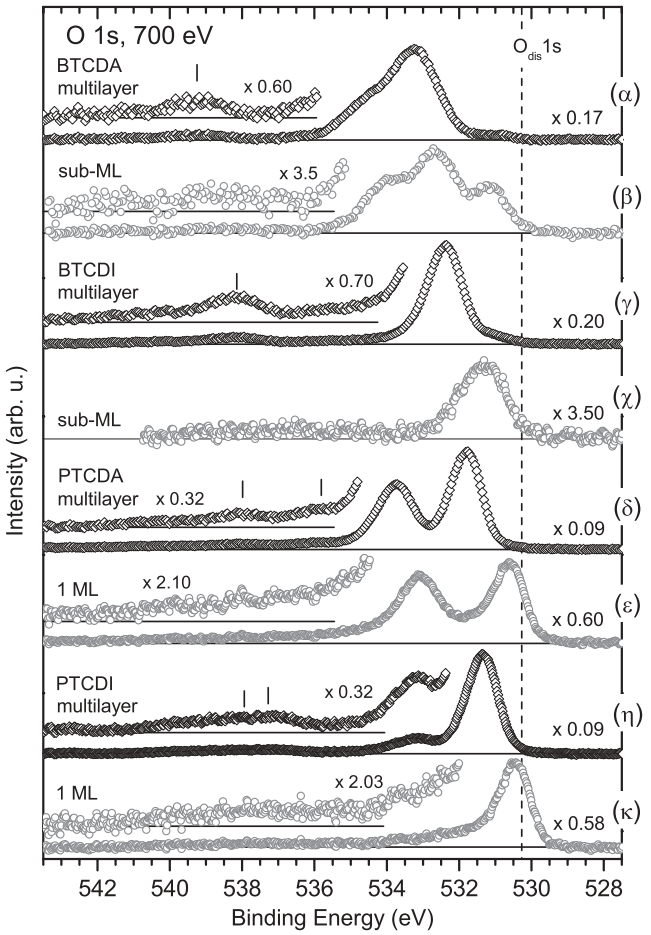

FIG. 4. Comparison of O 1*s* spectra of multilayer (black) and ML films (gray) of BTCDA (α,β), BTCDI (γ,χ), PTCDA (δ,ϵ), and PTCDI (η,κ) on Ag(111). The satellite signal is additionally shown on a $\times 3.5$ expanded intensity scale. The energy position of dissociated oxygen on Ag(111) is marked by a vertical line.[51,52]

level spectra are discussed briefly in the following, including some more detailed comments on the BTCDA and BTCDI spectra.

A. C 1*s* levels

The C 1*s* spectra are plotted in Fig. 1 with the satellite contributions being depicted additionally on a $\times 3.5$ expanded intensity scale for better visualization. The spectrum α of the BTCDA multilayer film consists of two distinct peaks at $E_B =$ 286.71 eV and 290.55 eV with 1.58 eV and 1.38 eV full width half maximum (FWHM), which can be attributed to the carbon species in the benzenelike ring (C_b) and in the functional group (C_f). The intensities of these peaks are in excellent agreement with the stoichiometric ratio 3 : 2.

The general signature of the C 1*s* spectrum γ of the BTCDI multilayer film is similar to that of spectrum α. The C_b 1s and C_f 1s signals are shifted to lower binding energy, namely to $E_B = 285.91$ eV and 289.17 eV with 0.83 eV and 0.88 eV FWHM. This chemical shift can be attributed to the lower electronegativity of the nitrogen atom in the BTCDI molecule compared to the bridging oxygen species in case of BTCDA. The peak areas are again in excellent agreement with the stoichiometric ratio 3 : 2. The fact that the main peaks are significantly narrower than in spectrum α may be due to smaller chemical differences between the different carbon species in case of BTCDI, smaller vibronic broadening, and less inhomogeneous broadening. The latter aspect is corroborated by the linear dichroism in NEXAFS spectroscopy, which indicates a homogeneous layer of flat-lying molecules only in case of BTCDI.[21]

The C 1*s* spectrum δ of the PTCDA multilayer film has been discussed previously in detail.[16,40] The C 1*s* spectrum η of the PTCDI multilayer film can be interpreted in analogy to δ.

Altogether, the multilayer data can be well understood. The main peaks correspond to signals from chemically different carbon species, and small, distinct features are observed, which are related to (shake-up) satellite excitations, in particular for the PTCDA and PTCDI films. Note that the intensity of the satellite contributions is higher for PTCDA and PTCDI than for BTCDA and BTCDI, which can be attributed to the size of the molecular π system and its capability to reorganize upon photoionization, as it has been discussed in detail for a series of polyacene molecules.[41]

TABLE I. Maxima positions in the C 1*s*, N 1*s*, and O 1*s* core level spectra of BTCDA, BTCDI, PTCDA, and PTCDI multilayer films and ML (ML) films on Ag(111) as indicated in Figs. 1–4.

Molecule	Layer	Level	Peak positions E_B (eV)				
BTCDA	multilayer	C 1*s*	286.71	290.55	292.7	–	–
		O 1*s*	533.2	534.5	539.3	∼541	–
	ML	C 1*s*	285.09	287.3	288.97	–	–
		O 1*s*	531.1	532.6	534.0	538.5	541.5
BTCDI	multilayer	C 1*s*	285.91	289.17	291.4	293.7	–
		N 1*s*	400.55	–	–	–	–
		O 1*s*	532.38	538.20	∼541	–	–
	ML	C 1*s*	284.82	287.48	288.60	291.5	–
		N 1*s*	398.37	399.93	–	–	–
		O 1*s*	531.20	–	–	–	–
PTCDA	multilayer	C 1*s*	285.00	286.94	288.52	289.96	–
		O 1*s*	531.81	533.73	535.9	537.9	540.6
	ML	C 1*s*	283.97	284.54	286.94	288.16	289.59
		O 1*s*	530.62	533.12	–	–	–
PTCDI	multilayer	C 1*s*	285.00	286.82	288.03	289.39	290.59
		N 1*s*	400.05	402.35	–	–	–
		O 1*s*	531.36	533.09	537.8	–	–
	ML	C 1*s*	283.97	284.53	286.43	287.6	288.9
		N 1*s*	397.91	399.46	401.01	–	–
		O 1*s*	530.44	–	–	–	–

The C 1*s* spectra β, χ, ε, and κ of the ML films differ significantly from the multilayer spectra. The spectral differences are smallest for BTCDA (rigid level shift of 1.6 eV) and increase in this series to PTCDI with differential chemical shifts and strong changes of the spectral signature being observed. This suggests that the adsorbate-substrate interaction is weakest for the BTCDA ML film and increases in this series to the PTCDI ML film.

Moreover, Fig. 2 indicates that the molecules are not dissociated as discussed in detail in Ref. 21 where it has also been shown that the molecules are laying flat on the surface. Hence, the trend in this series of core level spectra from the BTCDA to the PTCDI ML film is due to systematic variations of the adsorbate-substrate interaction. The following trends are striking in the C 1*s* spectra β, χ, ε, and κ:

(i) Differential chemical shifts are observed in particular for the spectra ε (PTCDA) and κ (PTCDI).

(ii) The energy position of the maximum of the first peak decreases from $E_B = 285.1$ eV (BTCDA) to 283.9 eV (PTCDI) and its leading edge becomes narrower.

(iii) The satellite structure is increasingly modified from β to κ. Particularly, in the spectra ε and κ a several eV broad tail contributes at the high-energy side of the double peak signature ($E_B = 283.97$ eV and 284.54 eV) of the perylene signal, and the satellite structure is significantly broadened.

Note that the high binding energy tailing in ε and κ resembles the signature of Doniach-Mahan-Šunjić line profiles in the core level spectra of metals[42–46] and of strongly adsorbed atoms or molecules.[12,26,47] Equivalent spectral features from adsorbates on metal surfaces have previously been related to plasmon excitations.[22,23] Therefore, the broadening of the satellite structure and the appearance of the high-energy tail are significant indications for metallic character of the adsorbate film.

B. N 1*s* and O 1*s* levels

The general findings with respect to the C 1*s* data are also reflected in the N 1*s* and O 1*s* spectra in Figs. 3 and 4. The energy position of the maximum of the peak at lowest binding energy decreases within this series of ML spectra, the satellite structure is strongly modified, and in case of PTCDA and PTCDI the satellite structure is significantly broadened and a several eV broad tail contributes at the high-energy side of the peaks. The N 1*s* spectra show the modification of the satellite structure unambiguously, because the N 1*s* signal originates from a single atomic species. Note that in both N 1*s* spectra, χ and κ, the intensity of the peak at lowest binding energy ($*$), the main peak, is much lower than the intensity of the first satellite peak, and the energy separation between the main peak and the first satellite is similar.

The O 1*s* spectrum β of the BTCDA ML film can be understood analogously. Several fit approaches have been applied. The best fit result is shown in Fig. 5(b). The spectrum is fitted by seven Voigt profiles with 0.15 eV Lorentzian width and several constraints, which reduces the number of free fit parameters to ten. In this approach it was assumed that each oxygen species, the bridging and the terminal oxygen, contributes two peaks to the triple peak feature, the main peak and a comparatively intense satellite. Both main peaks and both satellites are forced to the same width, and the energy separation between the main peaks and the satellites is constrained to 1.55 eV, which corresponds to the mean value of the energy separations in spectrum χ ($\Delta E = 1.5$ eV) and κ ($\Delta E = 1.6$ eV) in Fig. 3. Additional satellite contributions at higher binding energies are also taken into account and the overall intensity of the different contributions was constrained to the stoichiometric ratio 2 : 1. The good agreement of the fit results (continuous line) with the experimental data (circles)

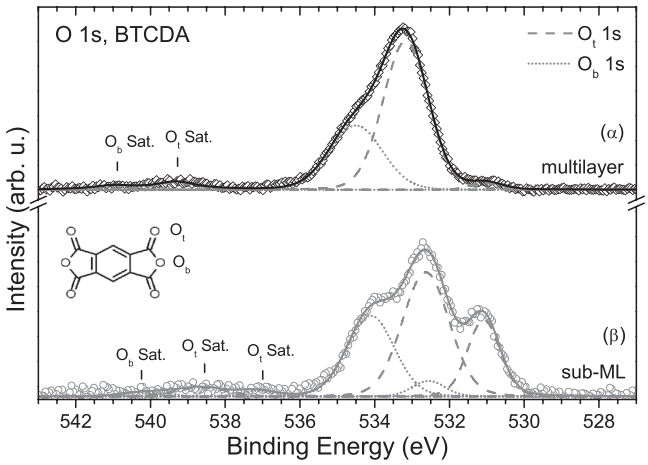

FIG. 5. Fit of the O 1s spectra of (a) spectrum α of a BTCDA multilayer film and (b) of spectrum β of a ML film on Ag(111). In (a) the overall intensities of the O_b 1s and the O_t 1s signals were constrained to the stoichiometric ratio 1 : 2, and the weak contribution of the ML signal was also taken into account (not shown here). See the text for more details on the fit in (b).

supports the assignment of the triple peak feature in the BTCDA ML spectrum to main peaks and satellite signals.

In summary we find the following general trends in relation to the core level spectra of the ML films: The adsorbate-substrate interaction is weakest for BTCDA sub-ML films and strongest for PTCDA and PTCDI ML films. The satellite structure in the core level spectra is particularly smeared out in case of the PTCDA/Ag(111) and PTCDI/Ag(111) ML films and a several eV broad tail is observed at the high-energy side of the dominant peaks, comparable to Doniach-Mahan-Šunjić line profiles in the core level spectra of metals or strongly chemisorbed adsorbates.[12,26,47] Moreover, distinct multipeak signatures are observed for the ML films, particularly for BTCDA/Ag(111) and BTCDI/Ag(111), which can be best explained by intense satellite excitations, similar to what has been found for weakly chemisorbed ML films of CO and N_2 on different metal surfaces[22,24,25,47,48,53–58] and carbonyl-transition-metal complexes.[59] In this context it has been referred to such spectral features as charge transfer satellites and giant satellites, respectively, because of their relation to adsorbate-substrate charge transfer and their extraordinary high intensity.

IV. MODEL FOR CHARGE TRANSFER SATELLITES

The interface interaction in general and the appearance of charge transfer satellites can be understood by considering the scenario of a two-level adsorbate with one core level c and one unoccupied valence level a, which is coupled to a metal substrate. After discussing the cases of no and finite adsorbate-substrate interaction the model is applied to the core level data shown above and related to the SINAM.[60,61]

A. Limit of no interface interaction

The principal behavior of the system can be understood by investigating the Hamiltonian

$$H = \epsilon_c n_c + [\epsilon_a - U_{ac}(1 - n_c)]n_a + \sum_k \epsilon_k n_k \qquad (1)$$

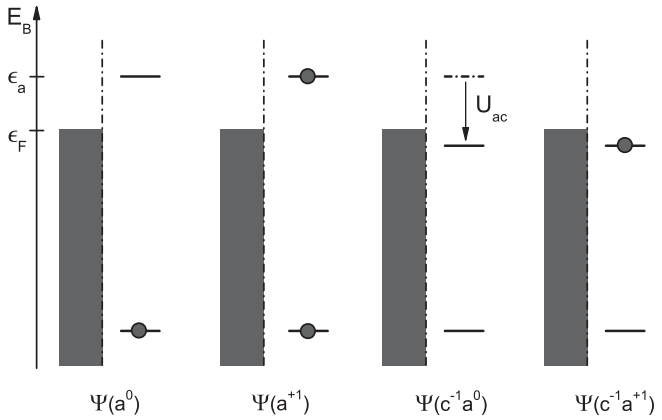

FIG. 6. Considered electronic configurations and eigenstates in case of vanishing adsorbate-substrate interaction ($V \to 0$), respectively.

with the energy of the unoccupied adsorbate valence level being ε_a, the energy of the core level being ϵ_c, and the occupation numbers n_a and n_c.[22–24] The third term corresponds to the substrate states. In the ground state the adsorbate level at the energy ε_a above the Fermi level ε_F is unoccupied. This electronic configuration is illustrated in Fig. 6 and described by the term a^0 in the following. Transferring an electron from the substrate to the adsorbate will cost the charge transfer energy $\Delta_{CT} = \varepsilon_a - \varepsilon_F$. Therefore, the total energy of the electronic configuration a^{+1} is Δ_{CT} higher than that of the ground state as it is indicated in the energy diagram in Fig. 7. It is convenient to refer the electronic energies to the Fermi level in the following, so that $\varepsilon_F = 0$ and $\Delta_{CT} = \varepsilon_a$.

Moreover, the creation of a core hole lowers the energy of the unoccupied adsorbate state by the energy U_{ac} due to Coulomb interaction with the core hole. For large U_{ac} the unoccupied adsorbate level can be pulled below the Fermi level as it is illustrated in Fig. 7 for the configuration $c^{-1}a^0$. In this case transferring an electron from the substrate to the

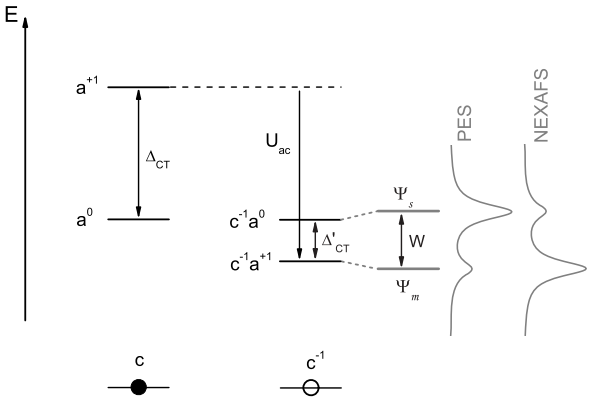

FIG. 7. Total energy of different electronic configurations. Left, black: Occupied adsorbate core level (c) and vanishing adsorbate-substrate coupling; center, black: Unoccupied adsorbate core level (c^{-1}) and vanishing adsorbate-substrate coupling; Right, gray: Unoccupied adsorbate core level (c^{-1}) and finite adsorbate-substrate coupling. The appearance of charge transfer satellites in the respective core level and NEXAFS spectrum is illustrated additionally.

adsorbate will lower the the total energy by $\Delta'_{CT} = \varepsilon_a - U_{ac}$. This is also illustrated in the energy diagram Fig. 7.

Furthermore, for the limit of vanishing interface interaction no interfacial charge transfer occurs. Hence, photoemission of a core electron leaves the remaining $(N-1)$ system in the configuration $c^{-1}a^0$. Therefore each core level contributes only to one single peak in the PE spectrum. Note that shake-up satellites are not taken into account by this approach, because the occupied valence states are neglected. This simplification is acceptable, as in the core level spectra of the multilayer films discussed above shake-up satellites contribute considerably less to the signal than the main peaks.

B. Finite interface interaction

The adsorbate-substrate coupling can be taken into account by approximating the eigenstates with a twofold basis set according to the approach by Sawatzky *et al.* in Ref. 27 for transition metal compounds. Particularly the ground state can be expressed as a linear combination of the eigenstates $\Psi(a^0)$ and $\Psi(a^{+1})$, which are illustrated in Fig. 6.

$$\Psi_1 = \sin\theta\Psi(a^0) + \cos\theta\Psi(a^{+1}) \tag{2}$$

$$\Psi_2 = \cos\theta\Psi(a^0) - \sin\theta\Psi(a^{+1}). \tag{3}$$

Here the mixing parameter is $0^\circ < \theta < 45^\circ$. Note that for the limit of vanishing interface interaction ($\theta \to 0^\circ$) the ground state is Ψ_2. The core excited states can be expressed analogously with respect to $\Psi(c^{-1}a^0)$, $\Psi(c^{-1}a^{+1})$ and the mixing parameter $45^\circ < \theta' < 90^\circ$.

$$\Psi_m = \cos\theta'\Psi(c^{-1}a^0) - \sin\theta'\Psi(c^{-1}a^{+1}) \tag{4}$$

$$\Psi_s = \sin\theta'\Psi(c^{-1}a^0) + \cos\theta'\Psi(c^{-1}a^{+1}) \tag{5}$$

This allows to derive the eigenvalues of H as a function of θ and θ' as lined out in Appendix. For $\theta' < 90^\circ$ the energy separation

$$W = E_s - E_m = \sqrt{\Delta'^2_{CT} + 4T'^2} \tag{6}$$

is larger than the charge transfer energy Δ'_{CT}. The contribution of the core excited states Ψ_m and Ψ_s to the core level spectrum can be estimated within the sudden approximation. According to the monopole selection rule for satellite transitions[62,63] their intensity depends on the direct overlap of the $N-1$ electron wave functions of the ground state and the excited states, namely the overlap of $\Psi_2(N-1)$ with $\Psi_l(N-1)$ and $\Psi_m(N-1)$.

$$\begin{aligned}\frac{I_s}{I_m} &= \frac{|\langle\Psi_l(N-1)|\Psi_2(N-1)\rangle|^2}{|\langle\Psi_m(N-1)|\Psi_2(N-1)\rangle|^2} \\ &= \left(\frac{\sin\theta'\cos\theta - \cos\theta'\sin\theta}{\cos\theta'\cos\theta + \sin\theta'\sin\theta}\right)^2 \\ &= \tan^2(\theta'-\theta).\end{aligned} \tag{7}$$

Consequently, the core level spectrum consists of a main peak with intensity I_m which corresponds to the core excited state of lowest energy E_m and a satellite with intensity I_s, which corresponds to the core excited state of energy E_s with the energy separation W.

These interrelations are illustrated on the right-hand side of Fig. 7, where it is assumed that $\Delta_{CT} = \epsilon_a > 0$ and $\Delta'_{CT} = (\epsilon_a - U_{ac}) < 0$.

C. Application to core level spectra

The striking satellite structures in the core level spectra of the BTCDA and BTCDI ML films can be evaluated with respect to this approach. The energy positions E_s, E_m and the intensities of the corresponding main peaks and satellites I_s, I_m are obtained from a peak fit analysis of the data as it is shown exemplarily in Fig. 5 for the O $1s$ spectrum of the BTCDA/Ag(111) ML film and listed in Table II. Entering these parameters into the system of equations (6), (7), (A4) allows to determine the parameters θ, θ', Δ'_{CT}, and T'.

As this system of equations is underdetermined various solutions are possible. However, the photoemission initial state is the same for all excitations of a particular sample (e.g., for photoemission of a O_b $1s$, O_t $1s$, C_b $1s$, and C_f $1s$ electron from the BTCDA sub-ML film). Consequently, for a particular ML film θ can only take values that satisfy relations (6), (7), (A4) for all core level signals at the same time. Table II shows the respective parameters for the core level data of the BTCDA and the BTCDI sub-ML films discussed above. For BTCDA, for example, $\theta' - \theta$ takes values between 57° and 73°. Consequently, it is $\theta \leqslant 17^\circ$ in the limit of $\theta' = 90^\circ$ and $\theta' - \theta = 73^\circ$ because θ and θ' have to satisfy $0^\circ \leqslant \theta \leqslant 45^\circ$ and $45^\circ \leqslant \theta' \leqslant 90^\circ$, and θ has to be the same for all core level signals of the BTCDA sub-ML film. This allows to narrow down the interval of allowed values for the other parameters as well.

Table II indicates that θ is small for the BTCDA sub-ML film as well as for the BTCDI sub-ML film. Consequently, the configuration mixing is small in the ground state, and hence the ground state can be associated with the configuration $\Psi_2 \simeq \Psi(a^0)$. This implies that no adsorbate-substrate charge transfer occurs in agreement with the valence data in Fig. 9. The valence spectrum β of the BTCDA sub-ML film, namely, resembles the spectrum α of the multilayer film except for minor differences in the fine structure, which indicates that the LUMO[76] is completely unoccupied in case of the BTCDA sub-ML film. Hence, the following discussion concentrates on the scenario $\theta \to \theta_{min}$.

Furthermore, one expects with respect to the discussion in Sec. IV B that the adsorbate-substrate charge transfer increases the further the previously unoccupied molecular level is pulled below the Fermi level ($U_{ac} > \varepsilon_a$). This implies that the contribution of $\Psi(c^{-1}a^{+1})$ to the eigenstate Ψ_m increases and the contribution of $\Psi(c^{-1}a^0)$ decreases with increasing $|\Delta'_{CT}|$. This behavior is illustrated in Fig. 8 for the parameters in Table II. The contribution

$$\begin{aligned}\langle n_{gs}\rangle &= \frac{|\langle\Psi(c^{-1}a^0)|\Psi_m\rangle|^2}{|\langle\Psi_m|\Psi_m\rangle|^2} \\ &= \cos^2\theta'\end{aligned} \tag{8}$$

is plotted with respect to the charge transfer energy Δ'_{CT}. The solid and dotted lines in Fig. 8 indicate all solutions for the parameters $\theta'_{min} \leqslant \theta' \leqslant \theta'_{max}$ and $\Delta'_{CT,min} \leqslant \Delta'_{CT} \leqslant \Delta'_{CT,max}$ listed in Table II. The circles mark the values for $\theta = \theta_{min}$ and $\theta' = \theta'_{min}$, respectively. This illustrates that for small

TABLE II. Parameters of the model for charge transfer satellites discussed in Sec. IV B for BTCDA and BTCDI ML films on Ag(111). It is indicated from the left to the right: The core level, the energy position of the satellite E_s, and the main peak E_m, together with the respective energy difference W and the intensity ratio I_s/I_m from the peak areas according to a peak fit analysis (not shown here). The difference in configuration mixing $\theta' - \theta$ was calculated with the relation (7) with $0^\circ < \theta < 45^\circ$ and $45^\circ < \theta' < 90^\circ$. From the comparison of $\theta' - \theta$ for different core levels the range of θ and θ' can be narrowed down as discussed in the text. The charge transfer energy Δ'_{CT} and the off–diagonal element T of the Hamiltonian can be estimated from θ' using the relations (6) and (A4).

Molecule	Core level	E_s(eV)	E_m(eV)	W (eV)	I_s/I_m	$\theta' - \theta$	θ	θ'	Δ'_{CT} (eV)	T (eV)
BTCDA	O_t 1s	532.63	531.08	1.55	2.3	57°	$\theta \leqslant 17^\circ$	$57^\circ \leqslant \cdots \leqslant 74^\circ$	$-1.36 \leqslant \cdots \leqslant -0.65$	$0.42 \leqslant \cdots \leqslant 0.73$
	O_b 1s	534.10	532.55	1.55	7.4	70°		$64^\circ \leqslant \cdots \leqslant 87^\circ$	$-1.55 \leqslant \cdots \leqslant -0.95$	$0.00 \leqslant \cdots \leqslant 0.61$
	C_C 1s	285.1	284.1	1.0	11	73°		$73^\circ \leqslant \cdots \leqslant 90^\circ$	$-1.00 \leqslant \cdots \leqslant -0.83$	$0.00 \leqslant \cdots \leqslant 0.28$
	C_O 1s	289.0	287.3	1.7	$\geqslant 3$	$\geqslant 60^\circ$		$60^\circ \leqslant \cdots \leqslant 77^\circ$	$-1.53 \leqslant \cdots \leqslant -0.85$	$0.37 \leqslant \cdots \leqslant 0.74$
BTCDI	N 1s	399.9	398.4	1.5	1.7	53°	$13^\circ \leqslant \theta \leqslant 21^\circ$	$66^\circ \leqslant \cdots \leqslant 74^\circ$	$-1.27 \leqslant \cdots \leqslant -1.00$	$0.40 \leqslant \cdots \leqslant 0.56$
	O 1s	531.7	531.0	0.7	0.8	42°		$55^\circ \leqslant \cdots \leqslant 63^\circ$	$-0.41 \leqslant \cdots \leqslant 0.24$	$0.28 \leqslant \cdots \leqslant 0.33$
	C_C 1s	284.8	284.0	0.8	$\geqslant 7$	$\geqslant 69^\circ$		$82^\circ \leqslant \cdots \leqslant 90^\circ$	$-0.80 \leqslant \cdots \leqslant -0.77$	$0.00 \leqslant \cdots \leqslant 0.11$
	C_N 1s	288.6	287.5	1.1	~0.4	$\geqslant 32^\circ$		$45^\circ \leqslant \cdots \leqslant 53^\circ$	$-0.30 \leqslant \cdots \leqslant 0.00$	$0.53 \leqslant \cdots \leqslant 0.55$

charge transfer energy $|\Delta'_{CT}|$ the core excited states have large contributions of both electronic configurations, $c^{-1}a^0$ and $c^{-1}a^{+1}$. For large $|\Delta'_{CT}|$ the main peak of the PE signal can predominantly be associated with the electronic configuration $c^{-1}a^{+1}$ and the satellite with the configuration $c^{-1}a^0$.

D. Relation to single-impurity Newns-Anderson model

The general behavior of the model discussed above is compatible with equivalent considerations within the framework of the SINAM.[60,61,65] Considering weakly covalent interaction between the single-impurity state $|a\rangle$ and the continuum of substrate states $|k\rangle$ under the assumption of negligible correlation energy U_{aa} between the two electrons in $|a\rangle$, the Anderson Hamiltonian for the interface problem has the form[24,33,34,66]

$$H = \epsilon_c n_c + [\epsilon_a - U_{ac}(1 - n_c)]n_a + \sum_k \epsilon_k n_k + \sum_k (V_{ak} c_a^\dagger c_k + V_{ka} c_k^\dagger c_a), \quad (9)$$

with ϵ_k corresponding to the energy of the states $|k\rangle$ of the free electron gas, V_{ak} being the coupling parameter between $|k\rangle$ and the adsorbate level $|a\rangle$, and $c_a^\dagger$ and $c_k^\dagger$ being the respective creation operators. The coupling between the state $|a\rangle$ of the adsorbate with energy E_a and the states $|k\rangle$ of a free electron gas leads to a density distribution of adsorbate-substrate valence states $\rho_a(\epsilon)$, which is commonly referred to as virtual bound state. This is illustrated in Fig. 10(a). The density distribution of adsorbate states can be described by

$$\rho_a(\epsilon) = \frac{1}{\pi} \frac{\Delta}{(\epsilon - E_a)^2 + \Delta^2}. \quad (10)$$

whereas in Fig. 10(a) the simplification $E_a = \epsilon_a$ is made. The width in energy Δ depends on the coupling parameter V and the electron density distribution of the free electron gas $\rho(\epsilon)$

$$\Delta = \pi \langle V^2 \rangle_{av} \rho(\epsilon). \quad (11)$$

Under the assumption that this density distribution of adsorbate-substrate states is only weakly modified by the core hole as illustrated in Figs. 10(b) and 10(c) one can estimate the charge transfer for a given Coulomb interaction U_{ac}. In a further approximation it is assumed that the core excited state of lowest energy (Ψ_m) corresponds to thermal equilibrium so that all states below the Fermi level are occupied due to adsorbate-substrate charge transfer as illustrated in Fig. 10(c). Then the amount of charge transferred from the substrate to the adsorbate can be determined by integrating the density distribution of adsorbate-substrate states $\rho_a(\epsilon + U_{ac})$ up to the Fermi level,

$$\langle n_a \rangle = \int_{-\infty}^{\epsilon_F} \rho_a(\epsilon + U_{ac})\, d\epsilon = \frac{1}{\pi} \arctan\left(\frac{-\Delta'_{CT}}{\Delta}\right) + 0.5. \quad (12)$$

This allows to relate the parameters of the SINAM directly to the model discussed in Sec. IV B. In particular $\langle n_a \rangle$ can

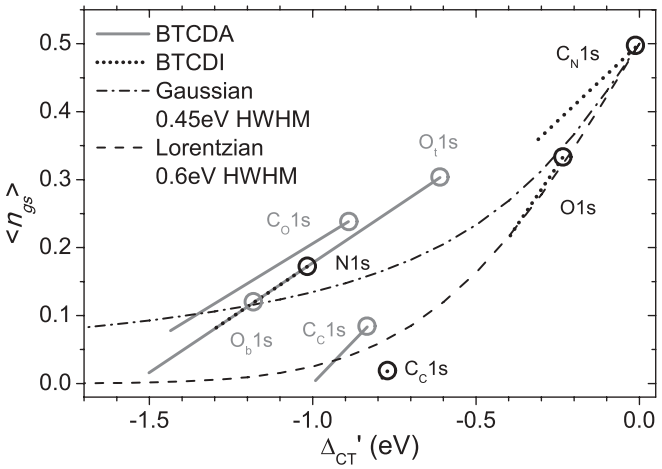

FIG. 8. Configuration mixing for the main peak of different core level signals from the BTCDI and BTCDA ML films. The contribution of the ground-state configuration $\langle n_{gs} \rangle = \cos^2 \theta'$ to each main peak is plotted over the charge transfer energy Δ'_{CT} for the values $\theta'_{min} \leqslant \theta' \leqslant \theta'_{max}$ given in Table II. The circles correspond to the situation $\theta' = \theta'_{min}$. Additionally, two simplified scenarios are indicated as discussed in Sec. IV D where the interface interaction leads to a density distribution of adsorbate-substrate states ρ_a which resembles a Lorentzian or a Gaussian profile.

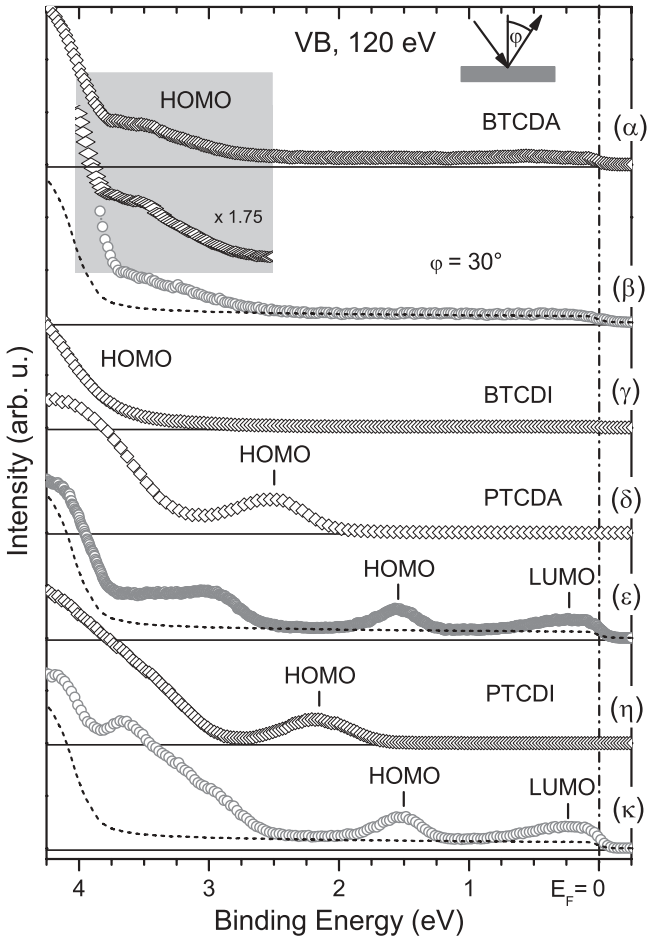

FIG. 9. Comparison of the angle-integrated valence band spectra of multilayer (black) and ML/sub–ML films (gray) of BTCDA (α,β), BTCDI (γ), PTCDA (δ,ε), and PTCDI (η,κ) on Ag(111). All spectra were recorded at normal emission geometry ($\varphi = 0°$), except for spectrum β, which was recorded at $\varphi = 30°$. The HOMO region of spectrum α (gray background) is also plotted on an enlarged intensity scale. In case of the ML data the angle-integrated spectrum of the clean silver substrate is additionally indicated (dashed lines). Note that according to Sec. IV the shift of the HOMO to lower binding energy in the spectra ε and κ compared to δ and η can at least partially be explained by the Coulomb interaction U_{ah} between the photohole and the occupied LUMO derived density of states as discussed in detail in Ref. 64.

be associated with the contribution of the the configuration $c^{-1}a^{+1}$ to the eigenstate Ψ_m according to

$$\Psi_m = \sqrt{1-\langle n_a\rangle}\ \Psi(c^{-1}a^{0}) \mp \sqrt{\langle n_a\rangle}\ \Psi(c^{-1}a^{+1}). \quad (13)$$

Then the comparison with (A3) and (8) yields $\langle n_a\rangle = \sin^2\theta'$ and $\langle n_{\rm gs}\rangle = 1 - \langle n_a\rangle$. The latter relation indicates that the unoccupied fraction of the density distribution of adsorbate-substrate states, namely in Fig. 10(c) the white area above the Fermi level, can be directly related to the contribution of the configuration $c^{-1}a^{0}$ to the eigenstate Ψ_m. Consequently, this simplified consideration of the SINAM provides another direct relation between $\langle n_{\rm gs}\rangle$ and the charge transfer energy $\Delta'_{\rm CT}$ in addition to the approach discussed in Sec. IV B. The further

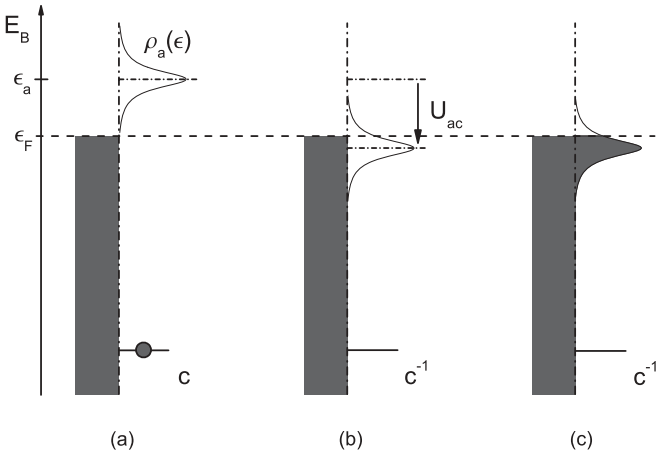

FIG. 10. Schematic illustration of (a) coupling between an unoccupied adsorbate valence level of energy ϵ_a and a continuum of substrate states with a density of adsorbate states $\rho_a(\epsilon)$ being formed, (b) the influence of the Coulomb interaction U_{ac} with a core hole c^{-1}, (c) an adsorbate-substrate charge transfer scenario.

the density distribution of adsorbate-substrate states is pulled below the Fermi level the smaller is $\langle n_{\rm gs}\rangle$.

This interrelation is indicated in Fig. 8 for two different density distributions of adsorbate-substrate states. The dashed line corresponds to the scenario where ρ_a is of Lorentzian shape with 0.6 eV half width half maximum (HWHM). The HWHM has been chosen with respect to the LUMO signal in the valence band spectra ε and κ of the PTCDA and PTCDI ML films in Fig. 9. As these signals resemble more a Gaussian than a Lorentzian profile the scenario where ρ_a is of Gaussian shape with 0.45 eV HWHM is indicated additionally by the dashed-dotted line.

Figure 8 shows that the evaluation of the core level spectra carried out in Sec. IV B agrees well with the simplified considerations in the framework of the SINAM. The further the density distribution of adsorbate-substrate states ρ_a is pulled below the Fermi level, the more it is occupied due to adsorbate-substrate charge transfer. However, there are also significant deviations in Fig. 8 between the trend of the BTCDA and BTCDI data compared to what is expected in relation to the simplified SINAM. In particular for the C_O 1s and the O_t 1s signal of the BTCDA film the values marked by circles are at significantly larger $\langle n_{\rm gs}\rangle$ than for the simplified SINAM. This can be attributed to the strong simplifications of the applied models.

The approach discussed in Sec. IV B reduces the complex reorganization of the electronic structure to the aspect of charge transfer from the substrate to an adsorbate state neglecting the formation of adsorbate-substrate hybrid states and the complex reorganization of the occupied states upon core excitation. The modification of these states upon core excitation, for example, can also contribute to the interfacial charge transfer and differential shifts between the satellite and the main peak. This is also interrelated with the creation of an image potential in the metal substrate and the reorganization of electronic states with predominantly molecular character. Similar simplifications have been introduced into the SINAM by assuming that the density distribution of adsorbate-substrate

states ρ_a is not modified by the core hole, except for being lowered in energy. Moreover, the system is obviously in a nonequilibrium state after core excitation, so that states above ε_F can be occupied, states below ε_F can be unoccupied, and electron-hole pairs can be formed directly at the Fermi level, as it will be discussed below in more detail. Therefore, the integral of ρ_a up to the Fermi level is only a first approximation of the adsorbate-substrate charge transfer. Nevertheless, Fig. 8 shows that the two models discussed here provide a similar trend despite their strong simplifications. This confirms that the applied models are compatible to each other and that they cover important aspects of the adsorbate-substrate interaction.

E. Near edge x-ray absorption fine structure spectroscopy

The validity of the concept discussed above is corroborated by the comparison between NEXAFS and core level spectra in Figs. 11 and 12. Figure 11(a) shows the C K-NEXAFS and C 1*s* core level spectra of a PTCDA/Ag(111) multilayer (top) and ML film (bottom). In case of the PTCDA multilayer film the C K-NEXAFS signal has a rich fine structure[16,67,68] and the low-energy onset is located at 283.3 eV at 0.5 eV lower energy than the onset of the C 1*s* spectrum (283.8 eV). A difference of 0.9 eV is observed analogously for the O 1*s* and O K-NEXAFS spectra of the PTCDA multilayer film in Fig. 11(b) with the onsets being located at 531.0 eV and 530.1 eV, respectively. Furthermore, Fig. 11 shows that for the ML film the low-energy onset of the NEXAFS and the core level spectra coincide in energy, and the C K-NEXAFS spectrum of the ML film has not such a sharp fine structure as the spectrum of the multilayer film.

This finding can be understood with respect to the energy diagram Fig. 7. For the limit of zero coupling (black) only one peak contributes to the core level and to the NEXAFS spectrum with the configuration $c^{-1}a^{0}$ corresponding to the photoemission final state and $c^{-1}a^{+1}$ to the final state of the NEXAFS transition under the assumption of appropriate

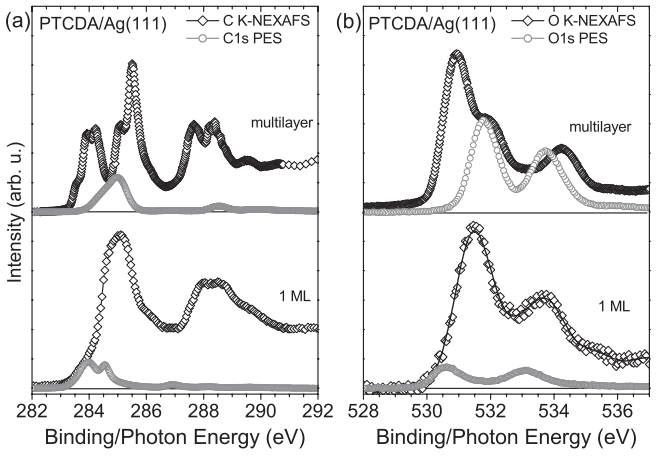

FIG. 11. (a) C 1*s* PES and C K-NEXAFS spectrum for the PTCDA/Ag(111) multilayer and ML film on Ag(111). (b) O 1*s* PES and O K-NEXAFS data for the PTCDA ML and multilayer film. All NEXAFS spectra were recorded with *p*-polarized x-ray light and a partial electron yield detector with 150 V and 300 V retarding voltage in case of the C K edge and the O K edge, respectively.

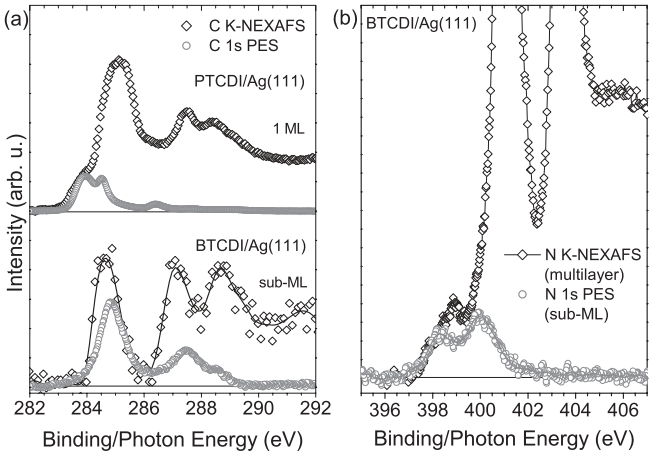

FIG. 12. (a) C 1*s* PES and C K-NEXAFS spectrum for a PTCDI ML film and a BTCDI sub-ML film. (b) N 1*s* spectrum for the BTCDI sub-ML film and N K-NEXAFS spectrum for the BTCDI multilayer film, where the signal at 398.9 eV might originate from the first ML. All NEXAFS spectra were recorded with *p*-polarized x-ray light and a partial electron yield detector.

symmetry of the core excited state $\Psi(c^{-1}a^{+1})$. In case of $\Delta\mathrm{CT}' < 0$, as shown in Fig. 7, the NEXAFS signal contributes at lower energy than the core level signal. Figure 11 indicates that this scenario applies for the PTCDA multilayer film with $\Delta'_{\mathrm{CT}} \sim -0.5$ eV and -0.9 eV for the C 1*s* and O 1*s* excitation, respectively. Consequently, the intermolecular interaction in the multilayer film is so weak that intermolecular charge transfer can be neglected.[69] Analogous results are also found for the C, O, and N K edges of BTCDA, BTCDI, and PTCDI multilayer films.

In case of significant adsorbate-substrate interaction the spectral contributions of the core excited states Ψ_l and Ψ_m depend on the contribution of $\Psi(c^{-1}a^{+1})$ to these states. Consequently, in case of considerable adsorbate-substrate coupling charge transfer satellites are expected in both, the core level PE and the NEXAFS spectra, as depicted in Fig. 7. This may be one reason for the loss of spectral fine structure in the C K-NEXAFS signal of the PTCDA ML film in Fig. 11(a). Moreover, the main peaks in the core level and in the NEXAFS spectra contribute at the same energy. Exactly this is observed for the PTCDA ML data in Fig. 11 (bottom).

In Fig. 12 the C 1*s* and N 1*s* spectra of the PTCDI and BTCDI ML films are compared to the respective C- and N K-NEXAFS spectra. The signature of the leading edge of the C 1*s* spectrum of the PTCDI/Ag(111) ML films in Fig. 12(a) resembles the signature of the corresponding C K-NEXAFS spectrum well, whereas the leading edge of the C 1*s* spectrum of the BTCDI/Ag(111) ML film is less steep. This can be understood with respect to the finding that in the case of BTCDI the adsorbate-substrate interaction is significantly weaker than for PTCDI. Hence, the configuration mixing is smaller for BTCDI than for PTCDI, and therefore the intensity of the main peak is smaller for BTCDI than for PTCDI. Consequently, the effect of adsorbate-substrate charge transfer depends on the strength of the adsorbate-substrate interaction.

Furthermore, the interpretation of the peak at 398.9 eV in the N K-NEXAFS spectrum of the BTCDI multilayer film in Fig. 12(b) is not unambiguous. It might be due to electronic transitions into the LUMO, which in principle are symmetry forbidden with respect to the finding for PTCDA and BTCDA.[67,69] However, the symmetry argument may be weakened due to vibronic coupling so that this transition contributes to the N K-NEXAFS spectrum of the BTCDI multilayer film. Another explanation might be that this signal originates from the first molecular layer and contributes to the multilayer spectrum because of a comparatively high film roughness in agreement with the O 1*s* spectrum γ in Fig. 4. Then this signal corresponds to transitions into the LUMO derived density distribution of adsorbate-substrate states. The fact that the leading edge of this NEXAFS signal agrees well with the leading edge of the N 1*s* signal of the ML film favors the latter interpretation.

V. DISCUSSION

Our investigation of the core level spectra of various ML films on Ag(111) indicates that adsorbate-substrate charge transfer upon core ionization plays a very significant role. Moreover, it has been shown that this effect increases with increasing adsorbate-substrate interaction. The approach discussed in Sec. IV B takes only two eigenstates Ψ_m, Ψ_s into account. It can be applied well to the core level data of BTCDA and BTCDI as in these spectra the satellites and the main peaks can be distinguished from each other. This is apparently not the case for the PTCDA and PTCDI ML data as the main peaks have a several eV broad tail at the high-energy edge, which is due to continuous satellite contributions as pointed out in Sec. III. These spectral features are similar to the continuous satellite structures known from the core level spectra of metals.[42–45] Their origin can be understood in the framework of the simplified SINAM discussed in Sec. IV D.

It has been illustrated by Fig. 10 that the adsorbate-substrate interaction can induce a density of adsorbate-substrate states, which can be cut by the Fermi level. The equilibrium condition depicted in Fig. 10(c) has the lowest total energy with all electronic states below the Fermi level being occupied and all states above being occupied. However, in case of a partially occupied density distribution of states the core ionization may be accompanied by the creation of electron-hole pairs directly at the Fermi level ε_F as it is known for core ionization of metal. It has been discussed previously by Doniach, Mahan, and Šunjić with respect to the core level spectra of metals, that this can lead to asymmetric line profiles and a several eV broad continuous tail at the high-binding-energy edge of the main peaks due to continuous satellite contributions.[42–45]

Analogous spectral features have been observed for the main peaks in the C 1*s*, O 1*s*, and N 1*s* spectra of the PTCDA and PTCDI ML films in Figs. 1, 3, and 4. They can be explained by the creation of electron-hole pairs with respect to the distribution of adsorbate-substrate states in analogy to what is known for the core ionization of metals or strongly chemisorbed adsorbates. The finding that this effect is considerably larger in case of strong adsorbate-substrate interaction can be understood with respect to relation (11). The stronger the adsorbate-substrate interaction the larger V and the larger the width Δ of the density distribution of adsorbate-substrate states ρ_a. Hence, the metallic character of the satellite structure increases with increasing adsorbate-substrate interaction because Δ can be understood in analogy to the width of the valence band in metals. Consequently, the simple two-level approach from Sec. IV B is well suited in case of intermediate adsorbate-substrate interaction and narrow Δ. However, in case of strong interaction and large Δ the adsorbate-interaction charge transfer can be interrelated with unoccupied states below ε_F, occupied states above ε_F, and electron-hole pairs at the Fermi level, which leads to asymmetric peak profiles and continuous satellite contributions. This aspect needs to be considered for the interpretation of core level spectra of strongly interacting adsorbates on metal surfaces. Gunnarsson and Schönhammer showed that the core level spectra of ML films from small adsorbates could be calculated well by taking these aspects into account.[22–24]

VI. SUMMARY AND CONCLUSION

We have studied some important fundamental aspects of the adsorbate-substrate interaction on noble metal surfaces. It has been shown that well-defined multilayer and ML films of intact adsorbates can be prepared on the Ag(111) surface with different adsorbate-substrate interaction strength. Our comprehensive PES and NEXAFS study indicates that adsorbate-substrate charge transfer upon core ionization plays a significant role. This effect can lead to intense charge transfer features in the core level spectra. Moreover, it increases with increasing adsorbate-substrate interaction and induces metallic character in the PE data. We applied the approach of Sawatky *et al*. for transition metal compounds to the interface problem which incorporates previous work by Gunnarsson and Schönhammer as well as Kotani, Asada, Sugano, and others. The charge transfer aspect can be described well by this approach in case of intermediate adsorbate-substrate interaction, namely for BTCDA/Ag(111) and BTCDI/Ag(111) ML films.

Moreover, asymmetric peak profiles and continuous satellite contributions are observed in case of strong adsorbate-substrate interaction, namely for PTCDA/Ag(111) and PTCDI/Ag(111) ML films. These spectral features can be explained with respect to adsorbate-substrate charge transfer and metallic character of the monolayer films in analogy to the work of Doniach, Mahan, and Šunjić on the core level spectra of metals and the work of Gunnarsson and Schönhammer on small adsorbates. The asymmetric peak profiles and continuous satellite contributions can be considered as indications for considerable metallic character or at least a very strong coupling between the adsorbate and the substrate. The conclusion that the first molecular layer for these two adsorbate systems has indeed metallic character can unambiguously be derived from the fact that the LUMO-derived density of substrate-adsorbate states is partly occupied (see Fig. 9 and Refs. 16 and 70). Note that the metallic character is a fundamental property of strongly interacting ML films on metal surfaces, which has also been studied by high-resolution low-energy electron loss spectroscopy, two-photoelectron photoemission spectroscopy, and resonant photoemission spectroscopy.[21,71–75] Hence our study

provides not only a systematic comparison of high-quality spectroscopic data from some organic model systems on silver, but also a detailed understanding of PES and NEXAFS spectra of molecule/metal interfaces, as well as insight into important fundamental interface properties.

ACKNOWLEDGMENTS

We thank the BESSY staff, M. Wießner and M. Scholz for support during the beamtimes as well as J. Ziroff, I. Kröger, C. Sauer, and S. Kera for stimulating discussions. This work was supported by BESSY, by the BMBF (Contracts No. 05K10WW2 and No. 03SF0356B), and by the DFG (GRK 1221).

APPENDIX

The energy difference between the eigenstates and the peak intensities can be derived by solving the eigenvalue problem of the Hamiltonian H for the twofold basis set as it has been shown in Ref. 27. The principal relations derived from this approach will be interpreted in the context of the interface problem in the following. For small overlap integrals ($\langle\Psi(a^0)|\Psi(a^{+1})\rangle \to 0$) the eigenvalues are

$$E_{1,2} = E_0 + \tfrac{1}{2}\Delta_{\mathrm{CT}} \pm \tfrac{1}{2}\sqrt{\Delta_{\mathrm{CT}}^2 + 4T^2} \tag{A1}$$

with $\Delta_{\mathrm{CT}} = \langle\Psi(a^{+1})|H|\Psi(a^{+1})\rangle - \langle\Psi(a^0)|H|\Psi(a^0)\rangle$ being the charge transfer energy in the limit of vanishing adsorbate-substrate coupling and $T = \langle\Psi(a^{+1})|H|\Psi(a^0)\rangle$ being the off-diagonal element of the hamiltonian matrix. Both are related to each other according to

$$\tan 2\theta = \frac{2T}{\Delta_{\mathrm{CT}}}. \tag{A2}$$

Consequently, $T \to 0$ in the limit of vanishing adsorbate-substrate coupling as $\theta \to 0^\circ$. Equivalent relations are obtained for the core excited states:

$$E_{s,m} = E_0' + \tfrac{1}{2}\Delta_{\mathrm{CT}}' \pm \tfrac{1}{2}\sqrt{\Delta_{\mathrm{CT}}'^2 + 4T'^2}. \tag{A3}$$

with $\Delta_{\mathrm{CT}}' = \langle\Psi(c^{-1}a^{+1})|H|\Psi(a^{+1})\rangle - \langle\Psi(c^{-1}a^0)|H|\Psi(a^0)\rangle$ being the charge transfer energy in the limit of vanishing adsorbate-substrate coupling. It is related to $T' = \langle\Psi(c^{-1}a^{+1})|H|\Psi(c^{-1}a^0)\rangle$ by

$$\tan 2\theta' = \frac{2T'}{\Delta_{\mathrm{CT}}'}. \tag{A4}$$

*Corresponding author: achim.schoell@physik.uni-wuerzburg.de

[1] F. S. Tautz, Prog. Surf. Sci. **82**, 479 (2007).
[2] N. Ueno and S. Kera, Prog. Surf. Sci. **83**, 490 (2008).
[3] H. Peisert, D. Kolacyak, and T. Chassé, J. Phys. Chem. C **113**, 19244 (2009).
[4] A. Hauschild, K. Karki, B. C. C. Cowie, M. Rohlfing, F. S. Tautz, and M. Sokolowski, Phys. Rev. Lett. **94**, 036106 (2005).
[5] A. Hauschild, R. Temirov, S. Soubatch, O. Bauer, A. Schöll, B. C. C. Cowie, T.-L. Lee, F. S. Tautz, and M. Sokolowski, Phys. Rev. B **81**, 125432 (2010).
[6] E. Umbach, Prog. Surf. Sci. **35**, 113 (1990).
[7] M. Häming, M. Greif, M. Wießner, A. Schöll, and F. Reinert, Surf. Sci. **604**, 1619 (2010).
[8] M. Häming, M. Greif, C. Sauer, A. Schöll, and F. Reinert, Phys. Rev. B **82**, 235432 (2010).
[9] S. Duhm, A. Gerlach, I. Salzmann, B. Bröker, R. Johnson, F. Schreiber, and N. Koch, Organic Electronics **9**, 111 (2008).
[10] L. Romaner, D. Nabok, P. Puschnig, E. Zojer, and C. Ambrosch-Draxl, New J. Phys. **11**, 053010 (2009).
[11] E. Umbach, S. Kulkarni, P. Feulner, and D. Menzel, Surf. Sci. **88**, 65 (1979).
[12] E. Umbach, Solid State Commun. **51**, 365 (1984).
[13] E. Umbach, M. Sokolowski, and R. Fink, Appl. Phys. A **63**, 565 (1996).
[14] U. Baston, M. Jung, and E. Umbach, J. Electron Spectrosc. Relat. Phenom. **77**, 75 (1996).
[15] D. Gador, Y. Zou, C. Buchberger, M. Bertram, R. Fink, and E. Umbach, J. Electron Spectrosc. Relat. Phenom. **103**, 523 (1999).
[16] Y. Zou, L. Kilian, A. Schöll, T. Schmidt, R. Fink, and E. Umbach, Surf. Sci. **600**, 1240 (2006).
[17] L. Kilian, A. Hauschild, R. Temirov, S. Soubatch, A. Schöll, A. Bendounan, F. Reinert, T.-L. Lee, F. S. Tautz, M. Sokolowski *et al.*, Phys. Rev. Lett. **100**, 136103 (2008).
[18] A. Schöll, L. Kilian, Y. Zou, J. Ziroff, S. Hame, F. Reinert, E. Umbach, and R. H. Fink, Science **329**, 303 (2010).
[19] A. Schöll, Y. Zou, T. Schmidt, R. Fink, and E. Umbach, J. Phys. Chem. B **108**, 14741 (2004).
[20] M. Häming, C. Scheuermann, A. Schöll, F. Reinert, and E. Umbach, J. Electron Spectrosc. Relat. Phenom. **174**, 59 (2009).
[21] M. Häming, Ph.D. thesis, Universität Würzburg, 2010.
[22] K. Schönhammer and O. Gunnarsson, Solid State Commun. **23**, 691 (1977).
[23] O. Gunnarsson and K. Schönhammer, Solid State Commun. **26**, 147 (1978).
[24] O. Gunnarsson and K. Schönhammer, Phys. Rev. Lett. **41**, 1608 (1978).
[25] J. Fuggle, E. Umbach, D. Menzel, K. Wandelt, and C. Brundle, Solid State Commun. **27**, 65 (1978).
[26] E. Umbach, Surf. Sci. **117**, 482 (1982).
[27] G. van der Laan, C. Westra, C. Haas, and G. A. Sawatzky, Phys. Rev. B **23**, 4369 (1981).
[28] S. Larsson, Chem. Phys. Lett. **32**, 401 (1975).
[29] R. Zimmermann, P. Steiner, R. Claessen, F. Reinert, and S. Hüfner, J. Electron Spectrosc. Relat. Phenom. **96**, 179 (1998).
[30] R. Zimmermann, R. Claessen, F. Reinert, P. Steiner, and S. Hüfner, J. Phys. **10**, 5697 (1998).
[31] R. Zimmermann, P. Steiner, R. Claessen, F. Reinert, S. Hüfner, P. Blaha, and P. Dufek, J. Phys. **11**, 1657 (1999).
[32] A. Kotani and Y. Toyozawa, J. Phys. Soc. Jpn. **35**, 1073 (1973).
[33] S. Asada and S. Sugano, J. Phys. Soc. J. **41**, 1291 (1976).
[34] S. Asada and S. Sugano, J. Phys. C **11**, 3911 (1978).

[35] A. Kotani and H. Ogasawara, J. Electron Spectrosc. Relat. Phenom. **86**, 65 (1997).
[36] E. Ilton and P. Bagus, Surf. Sci. **602**, 1114 (2008).
[37] P. Bagus, C. Nelin, E. Ilton, M. Baron, H. Abbott, E. Primorac, H. Kuhlenbeck, S. Shaikhutdinov, and H.-J. Freund, Chem. Phys. Lett. **487**, 237 (2010).
[38] D. Batchelor, T. Schmidt, R. Follath, C. Jung, R. Fink, M. Knupfer, A. Schöll, T. Noll, F. Siewert, B. Büchner *et al.*, Nucl. Instrum. Methods Phys. Res., Sect. A **575**, 470 (2007).
[39] A. Schöll, Y. Zou, T. Schmidt, R. Fink, and E. Umbach, J. Electron Spectrosc. Relat. Phenom. **129**, 1 (2003).
[40] A. Schöll, Y. Zou, M. Jung, T. Schmidt, R. Fink, and E. Umbach, J. Chem. Phys. **121**, 10260 (2004).
[41] M. Rocco, M. Häming, D. Batchelor, R. Fink, A. Schöll, and E. Umbach, J. Chem. Phys. **129**, 074702 (2008).
[42] S. Doniach and M. Sunjic, J. Phys. C **3**, 285 (1970).
[43] G. D. Mahan, Phys. Rev. B **2**, 4334 (1970).
[44] J. Dow and D. Franceschetti, Phys. Rev. Lett. **34**, 1320 (1975).
[45] G. Mahan, Phys. Rev. B **11**, 4814 (1975).
[46] J. C. Woicik, M. Yekutiel, E. J. Nelson, N. Jacobson, P. Pfalzer, M. Klemm, S. Horn, and L. Kronik, Phys. Rev. B **76**, 165101 (2007).
[47] E. Umbach, Ph.D. thesis, Technische Universität München, 1980.
[48] R. Masel, E. Umbach, J. Fuggle, and D. Menzel, Surf. Sci. **79**, 26 (1979).
[49] A. Hornung, D. Zemlyanov, M. Muhler, and G. Ertl, Surf. Sci. **600**, 370 (2006).
[50] C. Wäckerlin, D. Chylarecka, A. Kleibert, K. Müller, C. Iacovita, F. Nolting, T. Jung, and N. Ballav, Nature Commun. **1**, 61 (2010).
[51] X. Bao, M. Muhler, B. Pettinger, R. Schlögl, and G. Ertl, Catal. Lett. **22**, 215 (1993).
[52] X. Bao, M. Muhler, T. Schedel-Niedrig, and R. Schlögl, Phys. Rev. B **54**, 2249 (1996).
[53] J. Fuggle and D. Menzel, Vakuum–Technik **27**, 130 (1978).
[54] C. R. Brundle, P. S. Bagus, D. Menzel, and K. Hermann, Phys. Rev. B **24**, 7041 (1981).
[55] P. S. Bagus and K. Hermann, Surf. Sci. **89**, 588 (1979).
[56] P. S. Bagus, C. R. Brundle, K. Hermann, and D. Menzel, J. Electron Spectrosc. Relat. Phenom. **20**, 253 (1980).
[57] K. Hermann, P. S. Bagus, C. R. Brundle, and D. Menzel, Phys. Rev. B **24**, 7025 (1981).
[58] N. V. Dobrodey, L. S. Cederbaum, and F. Tarantelli, Phys. Rev. B **57**, 7340 (1998).
[59] E. W. Plummer, W. R. Salaneck, and J. S. Miller, Phys. Rev. B **18**, 1673 (1978).
[60] P. W. Anderson, Phys. Rev. **124**, 41 (1961).
[61] D. M. Newns, Phys. Rev. **178**, 1123 (1969).
[62] R. Manne and T. Åberg, Chem. Phys. Lett. **7**, 282 (1970).
[63] R. Martin, D. Shirley, and C. Fadley, *Electron Spectroscopy: Theory, Techniques and Applications*, Vol. 1 (Academic Press, Waltham, Massachusetts, 1978).
[64] C. Sauer, M. Wiessner, A. Schöll, and F. Reinert (unpublished).
[65] D. R. Hamann, Phys. Rev. B **2**, 1373 (1970).
[66] B. Gumhalter, J. Phys. C **10**, L219 (1977).
[67] A. Schöll, Y. Zou, D. Hübner, S. Urquhart, T. Schmidt, R. Fink, and E. Umbach, J. Chem. Phys. **123**, 044509 (2005).
[68] J. Taborski, P. Väterlein, H. Dietz, U. Zimmermann, and E. Umbach, J. Electron Spectrosc. Relat. Phenom. **75**, 129 (1995).
[69] F. Holch, Ph.D. thesis, Universität Würzburg, 2009.
[70] A. Bendounan, F. Forster, A. Schöll, D. Batchelor, J. Ziroff, E. Umbach, and F. Reinert, Surf. Sci. **601**, 4013 (2007).
[71] F. S. Tautz, M. Eremtchenko, J. Schaefer, M. Sokolowski, V. Shklover, K. Glöckler, and E. Umbach, Surf. Sci. **502-503**, 176 (2002).
[72] F. S. Tautz, M. Eremtchenko, J. Schaefer, M. Sokolowski, V. Shklover, and E. Umbach, Phys. Rev. B **65**, 125405 (2002).
[73] C. H. Schwalb, S. Sachs, M. Marks, A. Schöll, F. Reinert, E. Umbach, and U. Höfer, Phys. Rev. Lett. **101**, 146801 (2008).
[74] S. Sachs, C. Schwalb, M. Marks, A. Schöll, F. Reinert, E. Umbach, and U. Höfer, J. Chem. Phys. **131**, 144701 (2009).
[75] C. H. Schwalb, M. Marks, S. Sachs, A. Schöll, F. Reinert, E. Umbach, and U. Höfer, Eur. Phys. J. B **75**, 23 (2010).
[76] For the sake of simplicity we will use the terms HOMO and LUMO also for the respective states of the adsorbed molecules although the LUMO may not be unoccupied anymore but contributes to a density of adsorbate-substrate states.